Available online at www.CivileJournal.org

Civil Engineering Journal

Vol. 5, No. 4, April, 2019

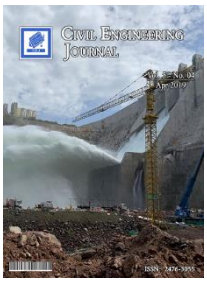

Effects of Near-fault Strong Ground Motions on Probabilistic Structural Seismic-induced Damages

Farzad Mirzaie Aminian [a], Ehsan Khojastehfar [b*], Hamid Ghanbari [a]

[a] *M.Sc. Student, Vali-e-Asr University of Rafsanjan, Rafsanjan, Iran.*

[b] *Assistant professor, Vali-e-Asr University of Rafsanjan, Rafsanjan, Iran.*

[c] *PhD Candidate, Shahid Bahonar University of Kerman, Kerman, Iran.*

Received 14 December 2018; Accepted 16 March 2019

Abstract

Seismic fragility curves measure induced levels of structural damage against strong ground motions of earthquakes, probabilistically. These curves play an important role in seismic performance assessment, seismic risk analysis and making rational decisions regarding seismic risk management of structures. It has been demonstrated that the calculated fragility curves of structures are changed while the structures are excited by near-field strong ground motions in comparison with far-field ones. The objective of this paper is to evaluate the extents of modification for various performance levels and variety of structural heights. To achieve this goal, Incremental Dynamic Analysis (IDA) method is applied to calculate seismic fragility curves. To investigate the effects of earthquake characteristics, two categories of strong ground motions are assumed through IDA method, i.e. near and far-field sets. To study the extent of modification for various heights of structures, 4 – 6 and 10 stories moment-resisting concrete frames are considered as case studies. Furthermore, to study the importance of involving near-field strong ground motions in seismic performance assessment of structures, the damage levels are considered as the renowned structural performance levels (i.e. Immediate Occupancy, Life Safety, Collapse Prevention and Sidesway Collapse). Achieved results show that the fragility curve of low-rise frame (i.e. 4-story case study) for IO limit state presents more probability of damage applying near-fault sets in comparison with far-fault set. Investigating fragility curves of the other performance levels (i.e. LS, CP and Collapse) and the higher frames, a straightforward conclusion, regarding probability of damage. To achieve the rational results for the higher frames, mean annual frequency of exceedance (MAFE) and probability of exceeding limit states in 50 years are calculated. MAFE is defined as the integration of structural fragility curve over seismic hazard curve. According to the achieved results for 6-story frame, if the structure is excited by near-field strong ground motions the probability of exceedance for LS, CP and collapse limit states in 50 years will be increased up to 11%, 2.4%, 0.7% and 0.4% respectively, comparing with the calculated probabilities while far-field strong ground motions are applied. On the other hand, while the 10-story case study is excited by near-field strong ground motions, the exceedance probability values for mentioned limit states decreases up to 20%, 5%, 4% and 4%, respectively. Consequently, it can be concluded that the lower is the height of the structure, the more will be the increment of probability of damage in the near-field conditions. Furthermore, this increment is much more for IO limit state in comparison with other limit states. These facts can be applied as a precaution for seismic design of low-rise structures, while they are located at the vicinity of active faults.

Keywords: Seismic Fragility Analysis; Near-fault Strong Ground Motions; Incremental Dynamic Analysis; Seismic Risk Analysis.

1. Introduction

Recently, Performance Based Earthquake Engineering (PBEE) is being evolved leading to the next generation performance based seismic design guideline [1]. As the first goal, the guideline is aimed to involve uncertainty sources

* Corresponding author: e.khojastehfar@vru.ac.ir

http://dx.doi.org/10.28991/cej-2019-03091289

in seismic design and assessment of structures through a consistent probabilistic method. Moreover, presentation of structural performance in terms of decision variables (DVs) which are comprehensible to different stakeholders, is desired. The most-widely used DVs are direct economic losses, downtime and casualties. Probabilistic seismic-induced damages to structures (i.e. fragility curves) is an influential step to calculate DVs. Among the others, inherent uncertainty and characteristics of earthquake strong ground motions are confirmed to be the most effective parameter on seismic-induced damages to the structures [2]. Consequently, several researches are devoted to the effects of strong ground motion uncertainties on seismic performance of structures [3-5]. In consequence of concentrated seismic excitation energy at the beginning part of near-fault strong ground motions, resultant probability of damage levels are changed in comparison with those of caused by far-fault strong ground motions. This fact motivates the needs for researches regarding effects of near-fault earthquakes on structural fragility curves.

Seismic-induced damages are illustrated by probabilistic fragility functions which play an important role in calculation of probabilistic seismic-induced risks (including economic losses, downtime and loss of lives). These functions present the probability of exceedance for damage limit states. According to this role, several methods have been proposed to compute comprehensive probabilistic damage functions. These methods are categorized into empirical, analytical and hybrid methods [6]. As the strong point of being an experiment-based approach, experienced damages caused by previous earthquakes are the main data contributor towards achieving fragility curves based on empirical methods [7]. On the other hand, scarcity of data, relevant to variety of damage levels and types of structures, provokes application of the analytical methods [6]. Through the analytical methods, responses of finite element models of assumed structures, against earthquake effects, provide the necessary data to calculate fragility curves. Earthquake effects are applied to the analytical models either by static pushover analysis (SPO) [8] or dynamic response history analysis (RHA) [9] methods. While SPO method makes incredible decrease in computational effort to calculate the fragility curves, the capability of RHA method to involve strong ground motion uncertainty in calculated fragility curves makes its results more inclusive. The most contributed uncertainty source, which affects seismic-induced damages to the structures, is confirmed to be the earthquake strong ground motion characteristics. This uncertainty source consists of exceedance probability of the strong ground motion intensities (such as peak ground acceleration (PGA), spectral acceleration (SA), …) and record-to-record variability; which includes frequency content, duration and other aspects of strong ground motions. While the former part is assimilated by the probabilistic seismic hazard analysis (PSHA), the latter is involved through the RHA of structures against selection of strong ground motions. Characteristics of the selected strong ground motions affect the resultant fragility functions [3].

Ground motions which are recorded at the vicinity of their causative faults show different characteristics comparing with those which are observed at the far distances [10]. This unique phenomena is experienced during the recent major earthquakes such as Northridge (1994), Kobe (1995) and Chi-Chi (1999), for each of these events, large amount of seismic-induced economic losses are triggered. The most distinguished features of near-fault strong ground motions, from the engineering viewpoint, are forward directivity and fling effects. Forward directivity occurs as the result of rupturing asperities on the fault towards the affected site with the same velocity as the propagated seismic wave velocity. On the other hand, the fling effect is the result of permanent ground displacement in the near-fault region [10]. Forward directivity effect is the origin of considerable seismic-induced economic losses to several facilities during recent earthquakes [10]. This effect is illustrated by existence of long-period pulses in velocity time-history of earthquakes. The mentioned pulse is quantified by the duration of time in which strong amplitude wave is transmitted, namely the pulse period. While several researches tried to detect forward directivity effects in strong ground motions by visual inspection of velocity time histories [11], quantification of the pulse period is desired in seismic performance analysis of structures affected by near-fault strong ground motions. To this end, Baker (2007) [12] proposed a method based on wavelet analysis. Through this method, the largest velocity pulse is extracted from the original velocity time history by wavelet transform. If the amplitude of the remaining motion is small relative to main ground motion, it will be classified as containing-pulse ground motion. Applying wavelet-based method, the pulse period is assumed to be the period of extracted waves. Calculation of the pulse period for earthquake records, through the suggested wavelet-based method, determines whether a given ground motion contains a velocity pulse or not. This fact enables selection of pulse-containing strong ground motions from libraries of recorded ground motions and studying the effects of pulse-like strong ground motions on seismic performance of structures.

Several researches were conducted to study the pulse-like strong ground motions effects on seismic behavior of structures. To mention some, Alavi and Krawinkler considered the effects of near-fault ground motions on seismic design of structures [13]. Through their research, they evaluated structural ductility demands as a design-aid parameter against near-fault effects. Response of high-rise buildings to near-fault strong ground motions were investigated by Anderson et al. [14]. They demonstrated that structures are imposed by more severe demands while being excited by near-fault strong ground motions, comparing with those imposed by far-field conditions. Kalkan and Kunnath [15] showed the dependency of structural seismic-induced responses on the ratio of fundamental structural period to ground motion pulse-period. Fragility analysis of retrofitted multicolumn bridge subjected to near- and far-fault strong ground motions is studied by Billah et al. [16], Dynamic Response of gravity dams is investigated by Zhang et al. [17]. Consequently,

importance of involving near-fault effects in seismic analysis of variety of structures has been well-defined among researches.

Regarding assessment of structural seismic performance against near-fault strong ground motions, several researches have been implemented. Effect of near-fault earthquakes on target displacement of structures, which is the structural performance indicator via FEMA 356 [18], is studied by Baltzopoulos et al. [19]. Seismic-induced damages, based on Park-Ang index [20], is investigated by Rofooii and Imani [21]. They demonstrated significant effects of near-fault strong ground motions on calculated damage indices for number of 3- and 9-story steel moment-resisting structures. Casey Champion and Liel [22] studied near-fault strong ground motion effects on collapse fragility curves of concrete structures. They have investigated 23 archetypical concrete moment-resisting buildings. They concluded that collapse capacities of frame affected by near-fault earthquakes are less than those affected by far-field earthquakes. The reduction of collapse capacity is demonstrated while the pulse period to fundamental period ratio is greater than two $T_p/T>2$. This fact is justified due to severe inelastic response and period elongation of structure during near-collapse state. Tzimas et al. studied collapse risk and residual drift performance of steel buildings equipped with post-tensioned moment-resisting frames and viscous damper in near-fault regions [23]. Number of recent studies investigated effects of near-fault strong ground motions on seismic-induced demand [24, 25], seismic design code [26] and direct displacement-based design methodology [27]. According to the mentioned researches regarding fragility assessment of structures against near-fault strong ground motions, they give emphasis to the collapse limit state. To the best of authors' knowledge, effects of pulse-like strong ground motions on calculated structural fragility curve for the other limit states (i.e. immediate occupancy (IO), life safety (LS) and collapse prevention (CP)) has not been investigated yet. Furthermore, the necessity of involving near-fault effects for variety of structures (i.e. low-rise, mid-rise and high-rise structures) has not been studied yet. The main goal of this research is to compare the effects of near-fault strong ground motions on seismic fragility curves for various limit states with the ones achieved by considering far-fault strong ground motions. Besides, it is intended to test which structures (in view of low-, mid- and high-rise structures) are mostly affected by considering near-fault strong ground motions.

To achieve these goals, three moment-resisting concrete frames are designed according to international code. Seismic fragility curves for various damage states are calculated by IDA method. Through this method, the structures are excited by number of strong ground motions with increasing intensities. To examine effects of near-fault strong ground motions, two distinguished record sets are applied by IDA. The first set consists of strong ground motions which do not contain velocity pulses, namely far-field set. The second set is the pulse-containing strong ground motions.. Besides, the fragility curves, for both ground motion scenarios, are presented for low-rise (4 stories), mid-rise (6 stories) and high-rise (10 stories) concrete moment frames.

2. Sampled Concrete Frames

2.1. Design Assumptions

In this research, three sampled moment-resisting concrete structures are considered as case studies. Number of stories is selected such as to be representative of low, mid and high-rise buildings. Structural design is implemented based on ACI318-05. Applied gravity loads and design assumptions are presented in Table 1. Seismic load is calculated based on national Iran seismic code (standard no. 2800). Typical plan of assumed structure is shown in Figure 1.

Table 1. Building design assumptions

Parameter	Value
Story Height	3.4 m
Span Width (Y-Direction)	5, 8, 4 and 5 m
Span Width (X-Direction)	5, 2.5,2.5 and 5 m
Damping Ratio	5%
Floor Dead load	580 kg/m^2
Floor Live load	200 kg/m^2
Roof Dead load	630 kg/m^2
Roof Live load	150 kg/m^2
Soil Type	III
Seismic Design Acceleration (A)	0.35
R_u	7
Steel yield strength	4000 kg/cm^2
Concrete compressive strength	350 kg/cm^2

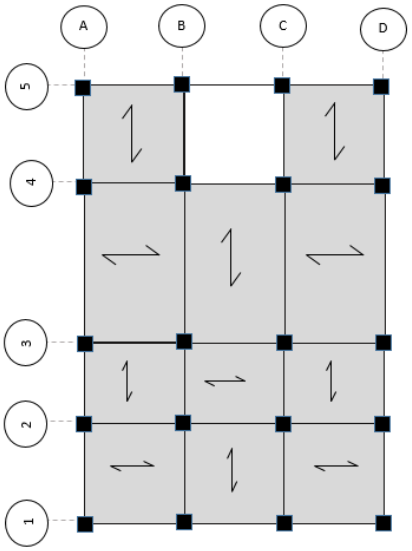

Figure 1. Typical Plan of Buildings

Symmetric configuration of structural plan lets two dimensional analysis of characteristic frames as representative for three dimensional seismic response of structures. Therefore, for each structure, frame no. B is modeled in OpenSees [28].

For brevity, result of structural design (including member dimensions, longitudinal and transverse reinforcement of structural members for 4-story frame is presented in Table 2.

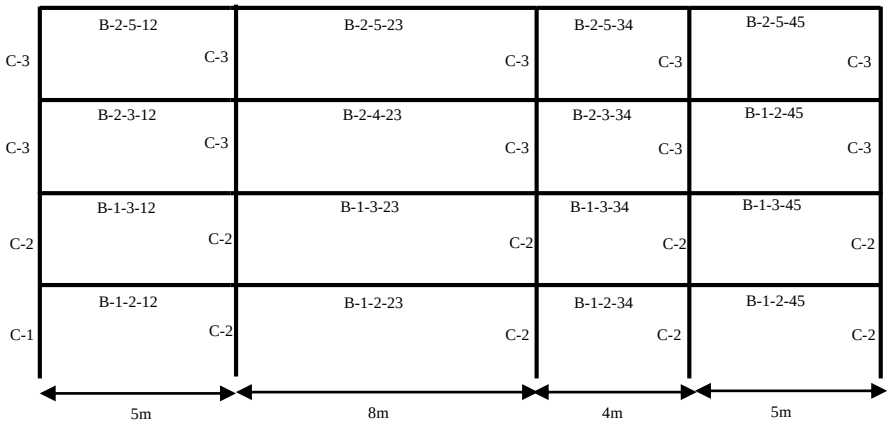

Figure 2. Frame No. B Sections for 4-story frame

Table 2. Designed sections for 4-story frame

Section Name	Dimension (mm^2)	Longitudinal Reinforcement	Transverse Reinforcement
C – 1	550 × 550	16 Φ 25	Φ 8 @ 75 mm
C – 2	450 × 450	16 Φ 22	Φ 8 @ 100 mm
C – 3	400 × 400	16 Φ 22	Φ 8 @ 125 mm
B – 1 – 2 – 12	400 × 600	5 Φ 25 (Bot) 5 Φ 25 (Top)	Φ 8 @ 100 mm
B – 2 – 4 – 12 , B – 2 – 4 – 23	400 × 400	6 Φ 25 (Bot) 3 Φ 25 (Top)	Φ 8 @ 150 mm
B – 2 – 5 – 12 , B – 2 – 5 – 34	400 × 400	4 Φ 25 (Bot) 3 Φ 25 (Top)	Φ 8 @ 200 mm
B – 1 – 2 – 23 , B – 1 – 2 – 34	400 × 600	5 Φ 25 (Bot) 3 Φ 25 (Top)	Φ 8 @ 200 mm
B – 1 – 2 – 23 ,B – 1 – 2 – 34	400 × 600	5 Φ 25 (Bot) 3 Φ 25 (Top)	Φ 8 @ 100 mm

B – 1 – 2 – 45	400 × 600	5 Φ 25 (Bot) 4 Φ 25 (Top)	Φ 8 @ 100 mm
B – 1 – 3 – 12 , B – 1 – 3 – 23	400 × 600	5 Φ 25 (Bot) 4 Φ 25 (Top)	Φ 8 @ 125 mm
B – 1 – 3 – 34 , B – 1 – 3 – 45	400 × 600	5 Φ 25 (Bot) 3 Φ 25 (Top)	Φ 8 @ 125 mm
B – 2 – 4 – 34 , B – 2 – 4 – 45	400 × 400	6 Φ 25 (Bot) 4 Φ 25 (Top)	Φ 8 @ 150 mm
B – 2 – 5 – 45	400 × 400	3 Φ 25 (Bot) 3 Φ 25 (Top)	Φ 8 @ 200 mm

2.2. Nonlinear Modeling

The sampled frames are modeled using nonlinear finite element software OpenSEES [28]. To evaluate nonlinear structural response to seismic actions the concentrated hinge plastic model is applied. This model consists of nonlinear rotational springs. These springs mimic the moment-rotation behavior of the connections. They are assigned at the beam ends. Moment-rotation behavior of nonlinear hinges is assumed as Modified Ibarra-Krawinkler model [29]. This model has been extensively used in previous researches to achieve seismic fragility curves of structures. Moment-rotation back-bone curve of Modified Ibarra-Krawinkler model is shown in Figure 3. Modeling parameters of concentrated hinges (i.e. effective stiffness, post-yield hardening strength ratio (M_c/M_y), θ_{Cap}^{tot}, θ_{Cap}^{pl} and θ_{pc}) are calculated based on formulations proposed by Haselton et al [30]. These formulations have been validated by comparing with various experimental studies [30]. Formulations of rotation modeling parameters are presented by Equations 1 to 3.

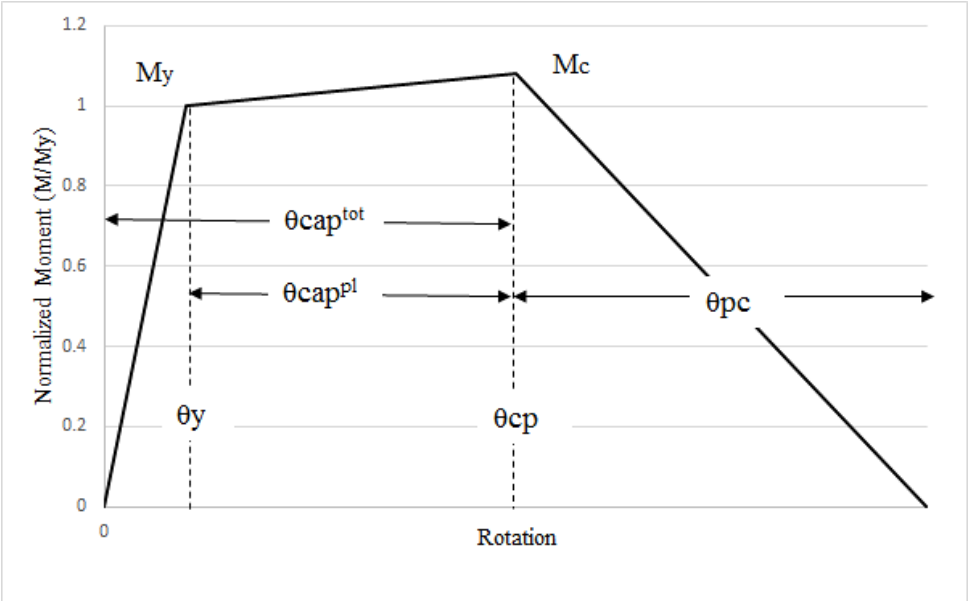

Figure 3. Moment-Rotation Backbone Curve

$$\theta_{cap,pl} = 0.13(1+0.55a_{sl})(0.13)^{\nu}(0.02+40\rho_{sh})^{0.65}(0.57)^{0.01C_{units}f'_c} \quad (1)$$

$$\theta_{cap,tot} = 0.14(1+0.4a_{sl})(0.19)^{\nu}(0.02+40\rho_{sh})^{0.54}(0.54)^{0.01C_{unit}f'_c} \quad (2)$$

$$\theta_{pc} = 0.76(0.031)^{\nu}(0.02+40\rho_{sh})^{1.02} \le 0.1 \quad (3)$$

Initial stiffness of the model is formulated according to decrease due to occurring crack in concrete elements. This decrement may be defined either by secant stiffness to the yield point or the secant stiffness to 40% of the yield moment. Stiffness is quantified as a fraction of the stiffness of the uncracked section (i.e. EI_g). The proposed formulation for secant stiffness to yield is applied in this research. This formulation is presented by Equation 4.

$$EI_y / EI_g = -0.07 + 0.59P / A_g f'_c + 0.07L_s / H \quad (4)$$

Post-yielding strength ratio of the structural beam elements is recommended as a constant value of 1.13 by Haselton et al. [30].

Parameters of above equations are defined in Table 3.

Table 3. Parameter Definition

Parameter	Definition
ρ_{sh}	Stirrup area ratio
ν	Axial load ratio ($P/A_g f'_c$)
f'_c	Concrete compressive strength (ksi)
a_{sl}	Slip term (1 for bond-slip and 0 for not bond-slip
C_{unit}	Constant to convert concrete strength unit (unity for ksi)

For each sampled frame, the modeling parameters are calculated according to the mentioned predictive equations. The resultant back-bone models are assigned to the nonlinear rotational springs. To evaluate structural seismic fragility curves the nonlinear models are excited by earthquake strong ground motions.

3. Sets of Strong Ground Motions

Three categories of strong ground motions, i.e. two sets of near-fault strong ground motions (NF-1 and NF-2 ground motions) and one set of far-field strong ground motions (FF ground motions), are considered for dynamic analysis of designed frames. NF1 set consists of 40 near-fault strong ground motions, which were used in SAC steel project [31]. NF2 set represents 40 near-fault strong ground motions, which were selected from PEER strong ground motion database. The earthquake selection was done in such a way to present records which include pulse effects. Two horizontal components of earthquakes are used for structural dynamic analysis. On the other hand, FF set includes 40 strong ground motions proposed by Krawinkler et al. [32] as Large Magnitude Short Distance (LMSR) dataset. Characteristics of near-field and far-field strong ground motions are presented in Tables 4 and 5, respectively.

Table 4. NF-1 and NF-2 Strong Ground Motions

NF – 1 Record set (PEER)						NF – 2 Record Sets (SAC)					
Event (Year)	**Station**	**M_w**	**Mechanism**	**T_p (Sec)**	**R (km)**	**Event (Year)**	**Station**	**M_w**	**Mechanism**	**T_p (Sec)**	**R (km)**
San Fernando (1971)	Pacoima Dam (upper left abut), 164	6.61	Reverse	1.638	1.81	Tabas (1978)	Tabas	7.35	Reverse	6.188	2.05
Tabas (1978)	Tabas	7.35	Reverse	6.188	2.05	Simulated	-	-	-	No pulse	
Coyote Lake (1979)	Gilroy Array #6	5.74	strike slip	1.232	3.11	Simulated	-	-	-	3.41	
Imperial Valley-06 (1979)	Agrarias	6.5	strike slip	2.338	0.65	Simulated	-	-	-	3.05	
Imperial Valley-06 (1979)	Brawley Airport	6.5	strike slip	4.396	10.42	Erzincan earthquake (1992)	Meteorological Station	6.69	Strike Slip	2.66	4.38
Irpinia Italy-01(1980)	Sturno (STN)	6.9	Normal	3.273	10.84	Lucerne (1980)	Lucerne	4.6	Normal	5.19	9.71
Westmorland (1981)	Parachute Test Site	5.9	strike slip	4.389	16.66	Northridge	Rinaldi Receiving	6.69	Reverse	1.24	6.5
Morgan Hill (1984)	Coyote Lake Dam - Southwest Abutment	6.19	Normal	1.071	10.84	Northridge	Sylmar - Converter	6.69	Reverse	2.43	5.35
Morgan Hill (1984)	Gilroy Array #6	6.19	Normal	1.23	9.78	Simulated	-	-	-	1.03	-
San Salvador (1986)	Geotech Investig Center	5.8	Strike-Slip	0.805	6.3	Kobe (1986)	Takatori	6.9	Strike Slip	1.62	1.47
Superstition Hills-02 (1987)	Parachute Test Site	6.54	Strike Slip	2.394	0.95	Simulated	-	-	-	No pulse	-
Loma Prieta (1989)	LGPC	6.93	Reverse-Oblique	**No-pulse**	**3.88**	Simulated	-	-	-	No pulse	-
Cape Mendocino (1992)	Cape Mendocino	7.01	Reverse	4.84	6.96	Simulated	-	-	-	2.92	-
Cape Mendocino (1992)	Petrolia	7.01	Reverse	2.996	8.18	Simulated	-	-	-	2.7	-
Landers (1992)	Lucerne	7.28	Strike Slip	5.124	2.19	Simulated	-	-	-	2.92	-
Northridge-01 (1994)	Pacoima Dam (downstr)	6.69	Reverse	0.588	7.01	Simulated	-	-	-	2.99	-
Northridge-03 (1994)	Rinaldi Receiving Sta	6.69	Reverse	1.246	6.5	Simulated	-	-	-	3.69	-

Kobe (1995)	KJMA	6.9	Strike Slip	1.092	0.96	Simulated	-	-	-	2.6	-
Kobe (1995)	Takatori	6.9	Strike Slip	1.554	1.47	Simulated	-	-	-	2.54	-
Loma Prieta (1989)	Los Gatos - Lexington Dam	6.93	Reverse-Oblique	1.568	5.02	Simulated	-	-	-	3.1	-

Table 5. Far-Field Strong Ground Motions

Event	Year	Mw	Station	R (km)	Mechanism	Event	Year	Mw	Station	R (km)	Mechanism
Loma Prieta	1989	6.9	Agnews State Hospital	28.2	Reverse-Oblique	Imperial Valley	1979	6.5	Niland Fire Station	35.9	Strike-Slip
Superstition Hills	1987	6.7	Brawley Airport	18.2	Strike-Slip	Northridge	1994	6.7	Hollywood Storage Ff	25.5	Reverse
Superstition Hills	1987	6.7	El Centro Imp. Co. Cent	13.9	Strike-Slip	Imperial Valley	1979	6.5	Plaster City	31.7	Strike-Slip
Superstition Hills	1987	6.7	Plaster City	21	Strike-Slip	Imperial Valley	1979	6.5	Cucapah	23.6	Strike-Slip
Superstition Hills	1987	6.7	Westmoreland Fire Station	13.3	Strike-Slip	Loma Prieta	1989	6.9	Halls Valley	31.6	Reverse-Oblique
Loma Prieta	1989	6.9	Capitola	14.5	Reverse-Oblique	Imperial Valley	1979	6.5	Westmoreland Fire Sta	15.1	Strike-Slip
Northridge	1994	6.7	La - Centinela	30.9	Reverse	Northridge	1994	6.7	Lake Hughes #1	36.3	Reverse
Northridge	1994	6.7	Canoga Park - Topanga Canyon	15.8	Reverse	Northridge	1994	6.7	Leona Valley #2	37.7	Reverse
Northridge	1994	6.7	La - Faring Rd	23.9	Reverse	Northridge	1994	6.7	Leona Valley #6	38.5	Reverse
Northridge	1994	6.7	La - Fletcher	29.5	Reverse	Northridge	1994	6.7	La-Pico & Sentous	32.7	Reverse
Loma Prieta	1989	6.9	Gilroy Array #3	14.4	Reverse-Oblique	Loma Prieta	1989	6.9	Salinas John & Work	32.6	Reverse-Oblique
Loma Prieta	1989	6.9	Gilroy Array #4	16.1	Reverse-Oblique	Loma Prieta	1989	6.9	Palo Alto Slac Lab	36.3	Reverse-Oblique
Northridge	1994	6.7	Glendale - Las Palmas	25.4	Reverse	Northridge	1994	6.7	Northridge - Saticoy	13.3	Reverse
Loma Prieta	1989	6.9	Gilroy Array #7	24.2	Reverse-Oblique	Northridge	1994	6.7	La - Saturn	30	Reverse
Imperial Valley	1979	6.5	Calipatria Fire Sta	23.8	Strike-Slip	Loma Prieta	1989	6.9	Sunnyvale Colton Ave	28.8	Reverse-Oblique
Imperial Valley	1979	6.5	Chihuahua	28.7	Strike-Slip	Northridge	1994	6.7	La - E Vernon	39.3	Reverse
Imperial Valley	1979	6.5	Compuertas	32.6	Strike-Slip	Imperial Valley	1979	6.5	El Centro Array #12	18.2	Strike-Slip
Imperial Valley	1979	6.5	El Centro Array #1	15.5	Strike-Slip	Imperial Valley	1979	6.5	El Centro Array #13	21.9	Strike-Slip
Northridge	1994	6.7	La Crescenta - New York	22.3	Reverse						

Existence of pulses in strong ground motion velocity time-history is one of the distinguished characteristics in near-fault ground motions. This factor is believed to have meaningful correlation with structural seismic-induced damages. In the present research, quantifying the predominant period of pulses is achieved by the algorithm proposed by Baker [12], based on wavelet transform of strong ground motion velocity time history. The calculated pulse periods for NF1 and NF2 sets are shown in Table 4. Based on Table 4, some of Near-Fault strong ground motions are categorized as no-pulse. This fact is either because of having no pulses in strong ground motion (i.e. no directivity effect in near fault strong ground motion) or inefficiency of proposed algorithm in view of calculation of related pulse periods. However, these records are excluded in structural damage analysis of structures against near-fault earthquakes.

4. Seismic Fragility Formulations

Structural damage states considered in the present study are corresponded to the renowned performance levels (i.e. Immediate Occupancy (IO), Life Safety (LS) and Collapse Prevention (CP)). These damage states are detected by maximum inter-story drift ratio (MIDR) of structures while being excited by strong ground motion of earthquakes. Based on FEMA 356 [18], the threshold of MIDR showing exceeding each damage states in moment-resisting concrete structures, are presented in Table 6.

Table 6. Damage states

Definition of Damage States			
Damage State	**Collapse Prevention**	**Life Safety**	**Immediate Occupancy**
Demand Value (MIDR)	4%	2%	1%

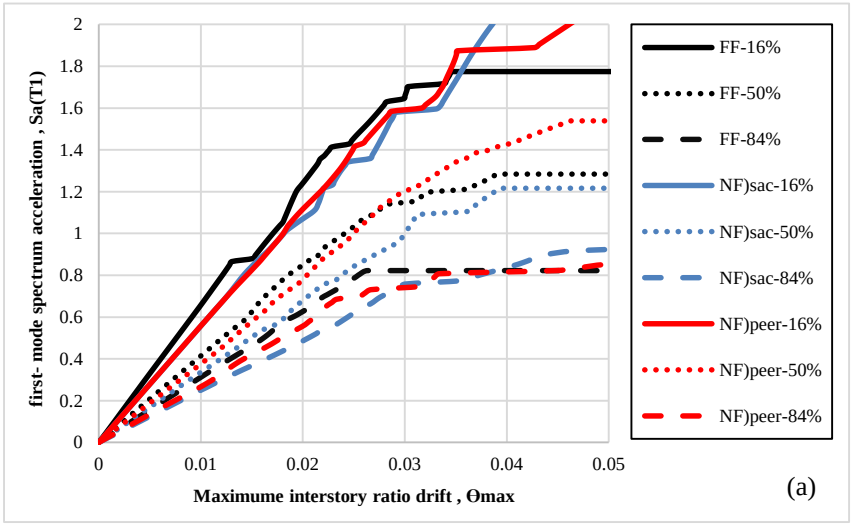

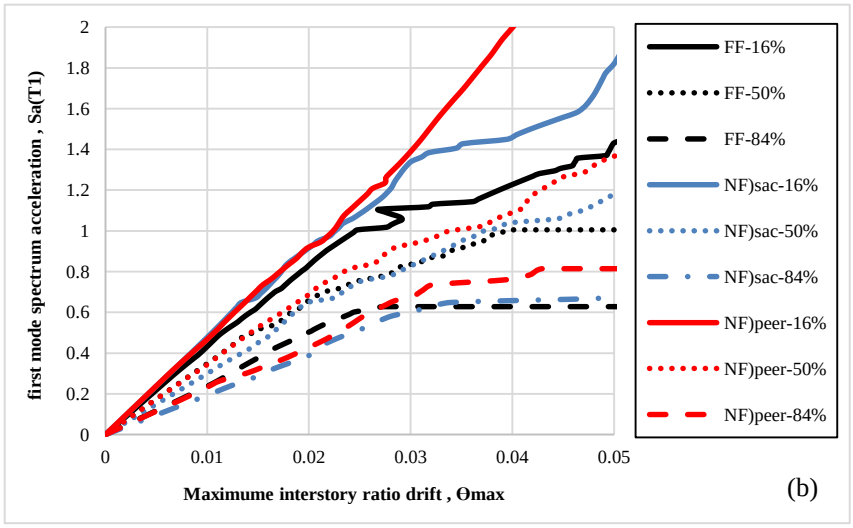

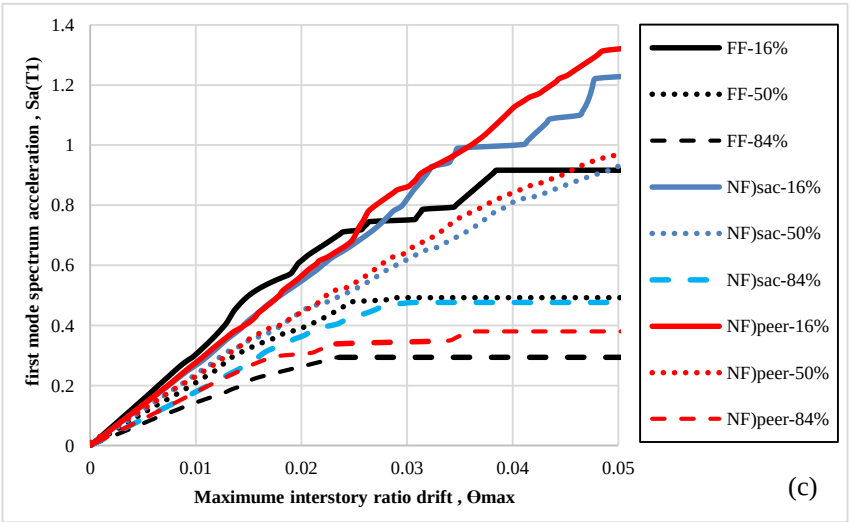

Figure 4. Summary of calculated IDA curves for 3 sets of strong ground motions: (a) 16%, 50% and 84% fractiles of IDA curves for 4-story sampled frame, (b) 16%, 50% and 84% fractiles of IDA curves for 6-story sampled frame and (c) 16%, 50% and 84% fractiles of IDA curves for 10-story sampled frame

Probabilistic damage curves, namely fragility curves, corresponding to each damage states are achieved by incremental dynamic analysis [31]. Through this method, the structure is excited by increasing intensities of strong ground motions. Plotting structural response parameter (i.e. engineering demand parameter (EDP)) versus ground motion intensity (i.e. Intensity Measure (IM)), presents IDA curves. Since the damage state thresholds are presented by maximum inter-story drift ratio (MIDR), this parameter is selected as EDP. Besides, towards having a reasonable comparison between near-field and far-field strong ground motion effects on seismic fragility curves, similar IM is selected for both cases. This parameter is selected as Spectral Acceleration corresponding to the fundamental period of the assumed structures. Summary of calculated IDA curves for the sampled frames considering three sets of strong ground motions are shown in Figure 4. Based on the achieved IDA curves, the SA values which correspond to each damage states (which are presented in Table 6) are predicted. The fragility curves, for each damage state, are calculated by fitting the Log-normal probability distribution to the predicted SA values. The least square method [3] has been proposed for fitting probability distribution to the achieved data from IDA curves. Through this method, mean and variance of probability distribution are calculated such as to present the minimum fitting error. The interpolation error is calculated based on difference between empirical probability (achieved by cumulative probability of each data) and analytical probability (achieved by cumulative distribution function). Summation of all differences over achieved data for each damage state presents corresponding error function. Achieved fragility curves for sampled structures are shown in Figures 5 to 7.

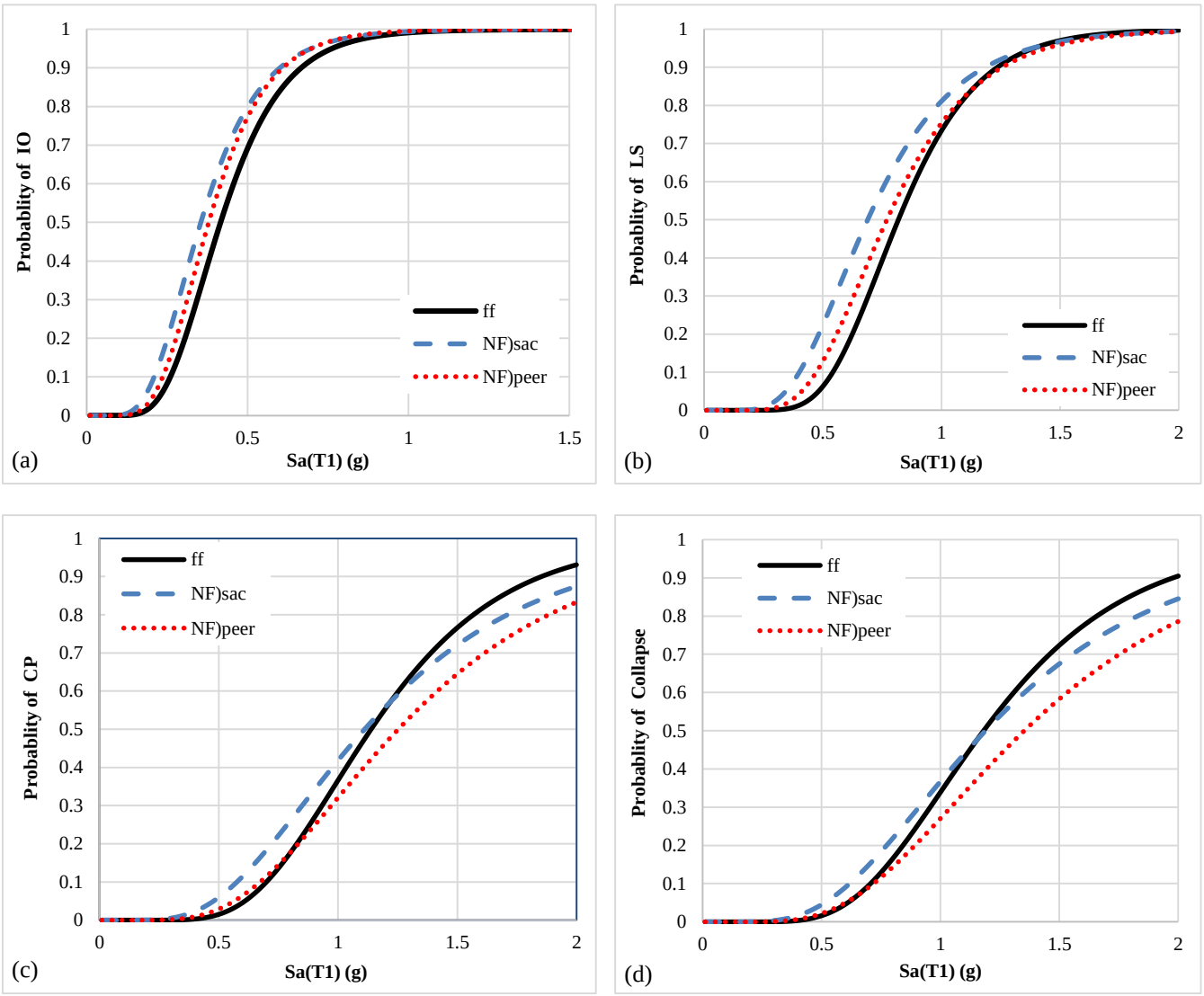

Figure 5. Fragility curves for 4-story sample frame: (a) IO limit state, (b) LS limit state, (c) CP limit state and (d) Collapse limit state

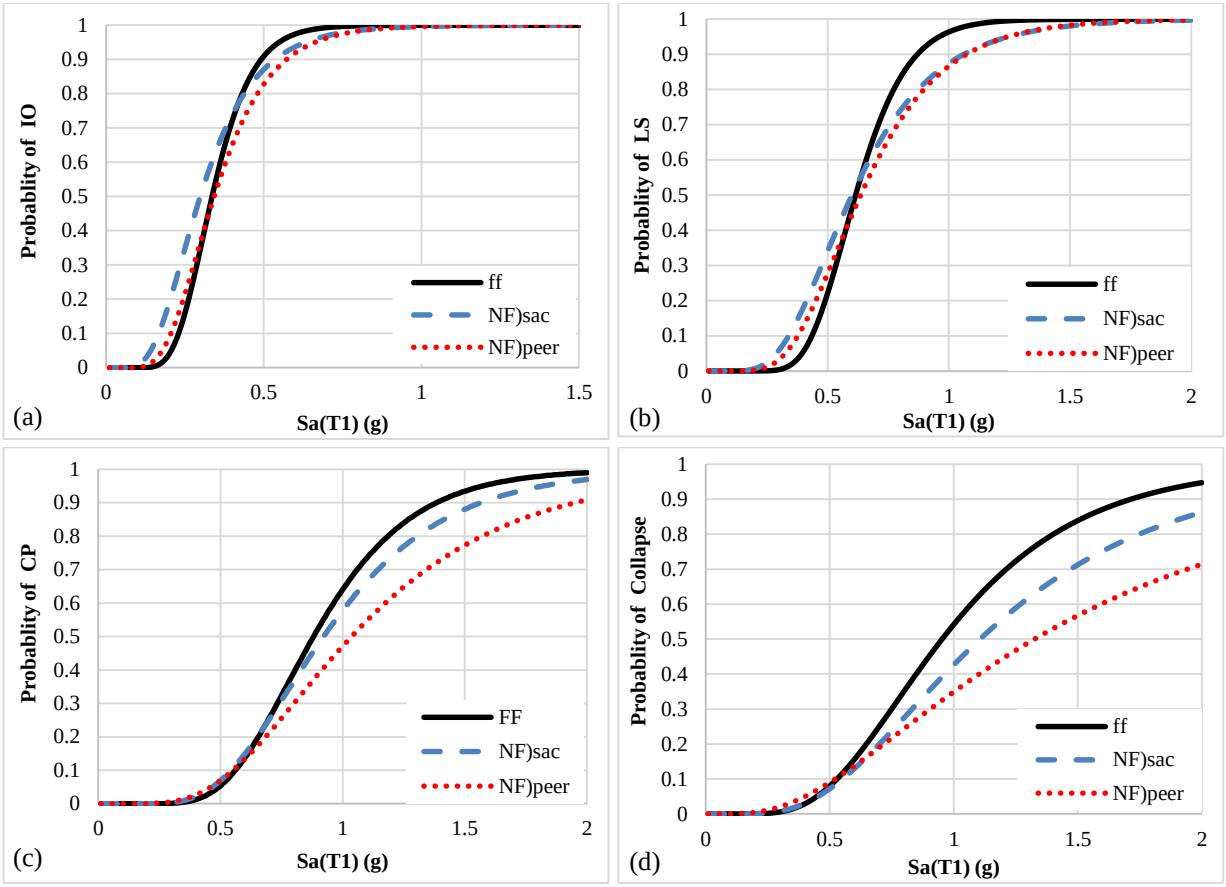

Figure 6. Fragility curves for 6-story sample frame: (a) IO limit state, (b) LS limit state, (c) CP limit state and (d) Collapse limit state

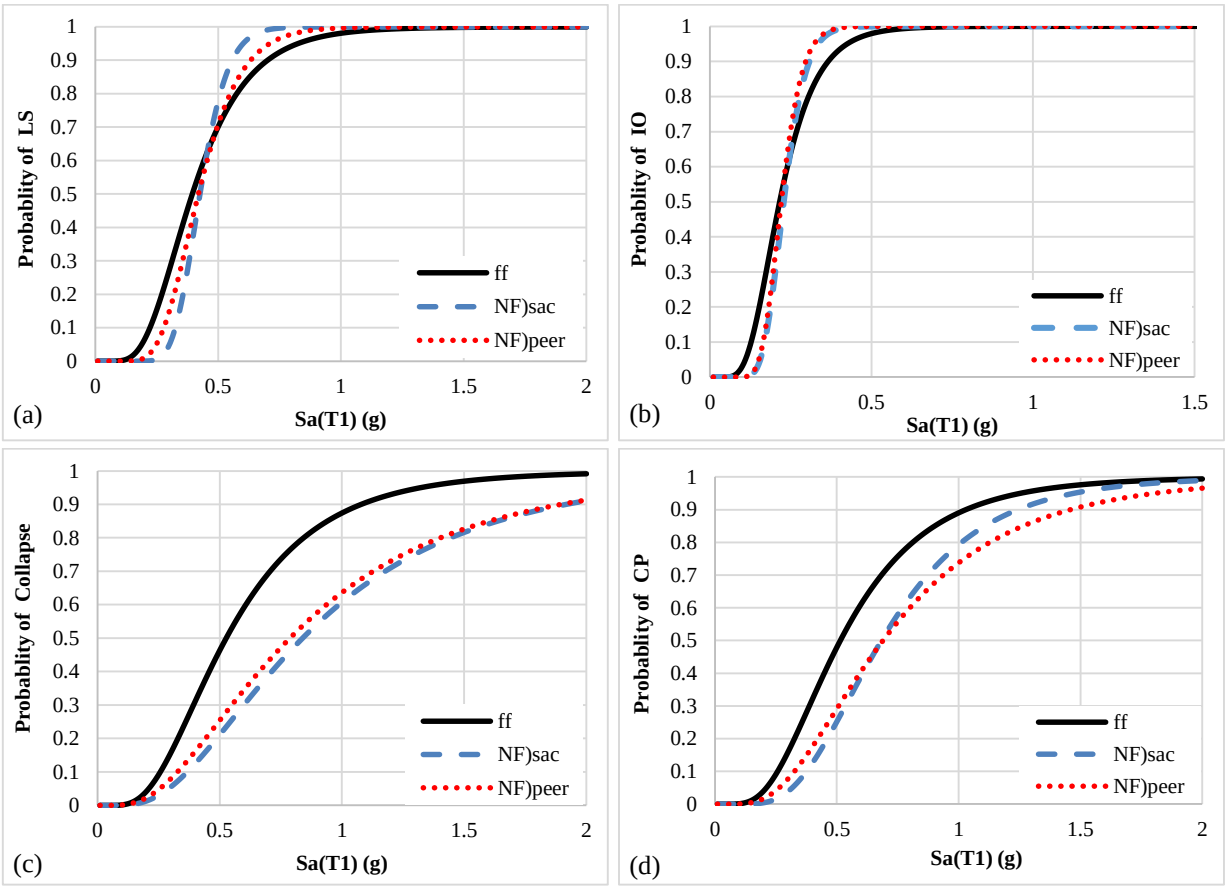

Figure 7. Fragility curves for 10-story sample frame: (a) IO limit state, (b) LS limit state, (c) CP limit state and (d) Collapse limit state

To calculate the mean annual frequency of exceedance (MAFE) for each damage state, integration of fragility curve multiplied by MAFE of IM over all IM values is implemented. The MAFE for each limit state is calculated based on Equation 5.

$$\lambda\left(Limit\ State\right)=\int_{IM} P\left(LS\mid IM=im\right)\left|d\lambda\left(im\right)\right| \quad (5)$$

To calculate the above integral, seismic hazard analysis of assumed site is needed. It has been shown in previous researches that MAFE of IM can be represented by regression of power function to the empirical data. Consequently, Equation 6 is used to calculate the MAFE of IM (i.e. λ(IM)).

$$\lambda\left(IM\right)=k_0\left(IM\right)^{-K} \quad (6)$$

In which k_0 and K are fitting coefficients, calculated based on nonlinear regression of Equation 4 to the seismic hazard data of the assumed structural site. Seismic hazard data are taken from Iran Seismic Hazard Analysis website.

Seismic risk of structures is defined as the probability of exceeding the damage states in 50 years. Based on the Poisson probability formulation, probability of exceeding a damage state in t years is represented by Equation 7.

$$P\left(LS\ in\ t\ years\right)=1-e^{-\lambda(LS)\,t} \quad (7)$$

In which, λ(LS) stands for MAFE of assumed limit state (calculated based on Equation 5).

Seismic risk values of the sampled frames are shown in Figures 8 to 10. Through these charts, risk values calculated for three sets of strong ground motions are presented.

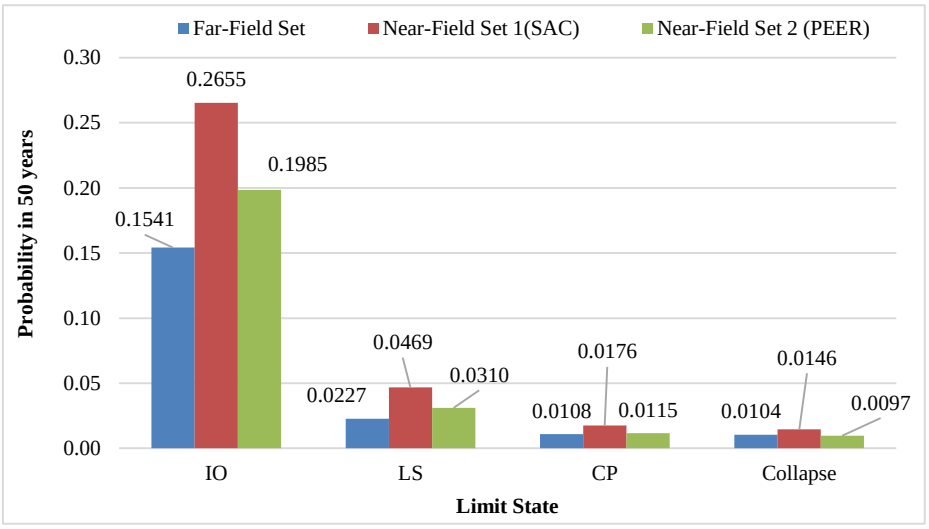

Figure 8. Exceedance probability of limit states for 4-story frame in 50 years considering three ground motion sets

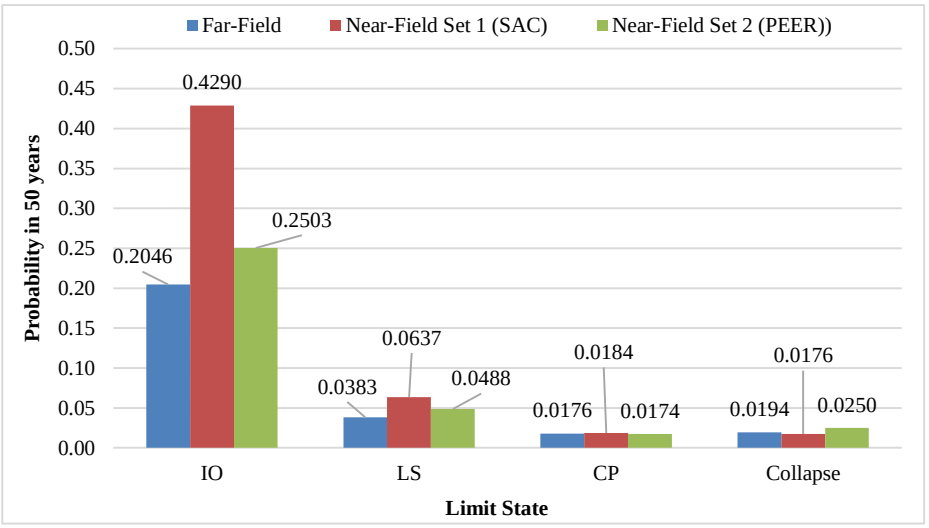

Figure 9. Exceedance probability of limit states for 6-story frame in 50 years considering three ground motion sets

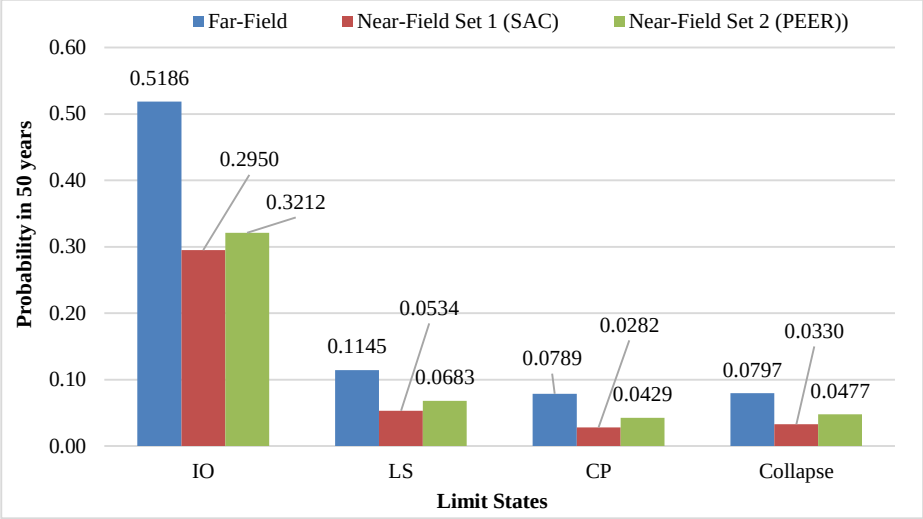

Figure 10. Exceedance probability of limit states for 10-story frame in 50 years considering three ground motion sets

5. Discussion

As it is illustrated in Figures 5, the fragility curves of the low-rise sampled frame (4-story frame in this paper) show more probabilities of damage for IO and LS limit states, while near-fault strong ground motion sets are applied. On the other hand, for 4-story frame, the result changes when fragility curves for CP and Collapse limit states are calculated. For low-rise structures which are located at the site prone to be affected by near-fault strong ground motions, this fact shows the necessity of involving near-fault strong ground motion while checking the IO and LS limit states. However, near-field fragility curves of the low-rise sampled frame for the CP and Collapse limit states, in some intensities, shows lower probabilities of damages, comparing with those of far-field damages. These conclusions are the consequence of the large amount of seismic-induced energy to the structures at the beginning of near-fault records. Consequently, the structure will enter IO and LS limit state at lower intensity while affected by the near-fault strong ground motions comparing with the far-field ones. On the other hand, CP and Collapse damage state are triggered when several hysteretic hinges are formed in structures. Consequently, probability of exceeding these limit states is rather correlated to the number of cycles in strong ground motions.

For the higher frames (6- and 10-story sampled frames in this study), comparison of damage probabilities calculated for the near-field and far-field strong ground motions in IO and LS limit states cannot be deduced just based on comparison of seismic fragility curves. Therefore, seismic-induced risks are calculated to present more consistent results.

Comparing fragility curves of 6-story frame for CP and Collapse limit states reveals that far-field strong ground motions show more probabilities of damages. Therefore, for mid-rise structures located at the sites prone to be affected by both near- and far-field strong ground motions, selection of design strong ground motions is suggested to be done with more care. This suggestion is made to insure to provide required structural protection against probable more seismic-induced damages which may be caused by far-field strong ground motions. Conversely, comparison of the fragility curves of high-rise sampled frame (10-story in this research) for CP and collapse shows that far-field strong ground motions will cause more severe damages.

Comparison of seismic-induced risks, for various damage states and for the 4-story and 6-story sampled frame, shows that near-fault induced risks are approximately twice than those obtained by FF strong ground motions for IO and LS limit states. On the other hand, for CP and Collapse limit state this difference is lower, although larger seismic risk are achieved while near-fault strong ground motions are applied. As it is expected by comparison of seismic fragility curves, seismic induced risks for 10 story frame are higher for FF set than NF1 and NF2 sets.

6. Conclusion

Effects of near-fault earthquake strong ground motions on seismic fragility analysis of concrete moment-resisting frames are investigated in this paper. To achieve this goal, three sampled moment-resisting frames are selected from three concrete structures. These structures are representative of various height classes (low-rise, mid-rise and high-rise structures). Two sets of near-fault strong ground motions, containing pulse effect, and one set of ordinary strong ground motions are chosen for nonlinear dynamic analysis of sampled frames. Seismic fragility analysis are implemented applying incremental dynamic analysis for four well-known damage states (Immediate Occupancy, Life Safety, Collapse

Prevention and Collapse). Furthermore, seismic-induced risk is calculated through integration of seismic fragility curves over probabilistic seismic hazard curves.

It was concluded that low-rise sampled frame shows more fragility and seismic risk for IO and LS limit states, while near-fault strong ground motions are applied. For higher structures and for the other limit states (i.e. CP and Collapse limit states), far-field strong ground motion set imposed more damages. Differences of seismic fragility and risk for NF1 and NF2, shows the substantial effect of ground motion pulse period to structural fundamental period ratio. This ratio is proved to be an important parameter in view of near-fault strong ground motion selection criteria in previous researches considering collapse limit state [33]. Proposed extension of this research consists of considering more sampled structures and strong ground motions. By this extension, quantitative criteria for selection of near-fault design strong ground motions for various limit states can be proposed.

7. Conflicts of Interest

The authors declare no conflict of interest.

8. References

[1] Applied Technology Council, and United States. Federal Emergency Management Agency. Quantification of building seismic performance factors. US Department of Homeland Security, FEMA, 2009.

[2] Kappos, Andreas. "Dynamic Loading and Design of Structures" (April 21, 2014). doi:10.1201/9781482272000.

[3] Kwon, Oh-Sung, and Amr Elnashai. "The Effect of Material and Ground Motion Uncertainty on the Seismic Vulnerability Curves of RC Structure." Engineering Structures 28, no. 2 (January 2006): 289–303. doi:10.1016/j.engstruct.2005.07.010.

[4] Shinozuka, Masanobu, M. Q. Feng, Jongheon Lee, and Toshihiko Naganuma. "Statistical Analysis of Fragility Curves." Journal of Engineering Mechanics 126, no. 12 (December 2000): 1224–1231. doi:10.1061/(asce)0733-9399(2000)126:12(1224).

[5] Celik, Ozan Cem, and Bruce R. Ellingwood. "Seismic Fragilities for Non-Ductile Reinforced Concrete Frames – Role of Aleatoric and Epistemic Uncertainties." Structural Safety 32, no. 1 (January 2010): 1–12. doi:10.1016/j.strusafe.2009.04.003.

[6] Calvi, G. Michele, Rui Pinho, Guido Magenes, Julian J. Bommer, L. Fernando Restrepo-Vélez, and Helen Crowley. "Development of seismic vulnerability assessment methodologies over the past 30 years." ISET journal of Earthquake Technology 43, no. 3 (2006): 75-104.

[7] Rossetto, T., and A. Elnashai. "Derivation of Vulnerability Functions for European-Type RC Structures Based on Observational Data." Engineering Structures 25, no. 10 (August 2003): 1241–1263. doi:10.1016/s0141-0296(03)00060-9.

[8] Baltzopoulos, Georgios, Roberto Baraschino, Iunio Iervolino, and Dimitrios Vamvatsikos. "SPO2FRAG: Software for Seismic Fragility Assessment Based on Static Pushover." Bulletin of Earthquake Engineering 15, no. 10 (May 8, 2017): 4399–4425. doi:10.1007/s10518-017-0145-3.

[9] Vamvatsikos, Dimitrios, and C. Allin Cornell. "Incremental Dynamic Analysis." Earthquake Engineering & Structural Dynamics 31, no. 3 (2002): 491–514. doi:10.1002/eqe.141.

[10] Mavroeidis, George P., and Apostolos S. Papageorgiou. "Near-source strong ground motion: characteristics and design issues." In Proc. of the Seventh US National Conf. on Earthquake Engineering (7NCEE), Boston, Massachusetts, vol. 21, no. 2, p. 25. 2002.

[11] Somerville, P. G., N. F. Smith, R. W. Graves, and N. A. Abrahamson. "Modification of Empirical Strong Ground Motion Attenuation Relations to Include the Amplitude and Duration Effects of Rupture Directivity." Seismological Research Letters 68, no. 1 (January 1, 1997): 199–222. doi:10.1785/gssrl.68.1.199.

[12] Baker, J. W. "Quantitative Classification of Near-Fault Ground Motions Using Wavelet Analysis." Bulletin of the Seismological Society of America 97, no. 5 (October 1, 2007): 1486–1501. doi:10.1785/0120060255.

[13] Alavi, Babak, and Helmut Krawinkler. "Consideration of near-fault ground motion effects in seismic design." In Proceedings of the 12th World Conference on Earthquake Engineering, p. 8. 2000.

[14] Anderson, J. C., V. V. Bertero, and R. D. Bertero. "Performance improvement of long period building structures subjected to severe pulse-type ground motions, Pacific Earthquake Engineering Research Center." University of California, Berkeley. Report no. PEEER-1999/09 (1999).

[15] Kalkan, Erol, and Sashi K. Kunnath. "Effects of Fling Step and Forward Directivity on Seismic Response of Buildings." Earthquake Spectra 22, no. 2 (May 2006): 367–390. doi:10.1193/1.2192560.

[16] Billah, A. H. M. Muntasir, M. Shahria Alam, and M. A. Rahman Bhuiyan. "Fragility Analysis of Retrofitted Multicolumn Bridge Bent Subjected to Near-Fault and Far-Field Ground Motion." Journal of Bridge Engineering 18, no. 10 (October 2013): 992–1004. doi:10.1061/(asce)be.1943-5592.0000452.

[17] Zhang, Sherong, and Gaohui Wang. “Effects of Near-Fault and Far-Fault Ground Motions on Nonlinear Dynamic Response and Seismic Damage of Concrete Gravity Dams.” Soil Dynamics and Earthquake Engineering 53 (October 2013): 217–229. doi:10.1016/j.soildyn.2013.07.014.

[18] Council, Building Seismic Safety. "Prestandard and commentary for the seismic rehabilitation of buildings." Report FEMA-356, Washington, DC (2000).

[19] Baltzopoulos, Georgios, Eugenio Chioccarelli, and Iunio Iervolino. “The Displacement Coefficient Method in Near-Source Conditions.” Earthquake Engineering & Structural Dynamics 44, no. 7 (October 20, 2014): 1015–1033. doi:10.1002/eqe.2497.

[20] Park, Y. J., A. H‐S. Ang, and Y. K. Wen. “Damage‐Limiting Aseismic Design of Buildings.” Earthquake Spectra 3, no. 1 (February 1987): 1‐26. doi:10.1193/1.1585416.

[21] Rofooei, Fayaz R., and Reza Imani. “Evaluating the Damage in Steel MRF Under Near Field Earthquakes from a Performance Based Design Viewpoint.” Procedia Engineering 14 (2011): 3111–3118. doi:10.1016/j.proeng.2011.07.391.

[22] Champion, Casey, and Abbie Liel. “The Effect of Near-Fault Directivity on Building Seismic Collapse Risk.” Earthquake Engineering & Structural Dynamics 41, no. 10 (January 12, 2012): 1391–1409. doi:10.1002/eqe.1188.

[23] Tzimas, A. S., G. S. Kamaris, T. L. Karavasilis, and C. Galasso. “Collapse Risk and Residual Drift Performance of Steel Buildings Using Post-Tensioned MRFs and Viscous Dampers in Near-Fault Regions.” Bulletin of Earthquake Engineering 14, no. 6 (March 18, 2016): 1643–1662. doi:10.1007/s10518-016-9898-3.

[24] Baltzopoulos, Georgios, Dimitrios Vamvatsikos, and Iunio Iervolino. “Analytical Modelling of Near-Source Pulse-Like Seismic Demand for Multi-Linear Backbone Oscillators.” Earthquake Engineering & Structural Dynamics 45, no. 11 (April 4, 2016): 1797–1815. doi:10.1002/eqe.2729.

[25] Güneş, Necmettin, and Zülfü Çınar Ulucan. “Nonlinear Dynamic Response of a Tall Building to Near-Fault Pulse-Like Ground Motions.” Bulletin of Earthquake Engineering (February 4, 2019). doi:10.1007/s10518-019-00570-y.

[26] Akkar, Sinan, Saed Moghimi, and Yalın Arıcı. “A Study on Major Seismological and Fault-Site Parameters Affecting Near-Fault Directivity Ground-Motion Demands for Strike-Slip Faulting for Their Possible Inclusion in Seismic Design Codes.” Soil Dynamics and Earthquake Engineering 104 (January 2018): 88–105. doi:10.1016/j.soildyn.2017.09.023.

[27] Lu, Yang, Iman Hajirasouliha, and Alec M. Marshall. “Direct Displacement-Based Seismic Design of Flexible-Base Structures Subjected to Pulse-Like Ground Motions.” Engineering Structures 168 (August 2018): 276–289. doi:10.1016/j.engstruct.2018.04.079.

[28] McKenna, Frank, Gregory L. Fenves, and Michael H. Scott. "Open system for earthquake engineering simulation." University of California, Berkeley, CA (2000).

[29] Ibarra, Luis F., Ricardo A. Medina, and Helmut Krawinkler. “Hysteretic Models That Incorporate Strength and Stiffness Deterioration.” Earthquake Engineering & Structural Dynamics 34, no. 12 (2005): 1489–1511. doi:10.1002/eqe.495.

[30] Haselton, Curt B., and Pacific Earthquake Engineering Research Center. Beam-column element model calibrated for predicting flexural response leading to global collapse of RC frame buildings. Pacific Earthquake Engineering Research Center, 2008.

[31] Somerville, Paul G. Development of ground motion time histories for phase 2 of the FEMA/SAC steel project. SAC Joint Venture, 1997.

[32] Krawinkler, H., R. Medina, and B. Alavi. “Seismic Drift and Ductility Demands and Their Dependence on Ground Motions.” Engineering Structures 25, no. 5 (April 2003): 637–653. doi:10.1016/s0141-0296(02)00174-8.

[33] Kohrangi, Mohsen, Dimitrios Vamvatsikos, and Paolo Bazzurro. “Pulse-Like Versus Non-Pulse-Like Ground Motion Records: Spectral Shape Comparisons and Record Selection Strategies.” Earthquake Engineering & Structural Dynamics 48, no. 1 (September 26, 2018): 46–64. doi:10.1002/eqe.3122.